Journal of Molecular Catalysis A: Chemical 337 (2011) 68–76

Contents lists available at ScienceDirect

Journal of Molecular Catalysis A: Chemical

journal homepage: www.elsevier.com/locate/molcata

Phototransformation of 4-nitrophenol using Pd phthalocyanines supported on single walled carbon nanotubes

Taofeek B. Ogunbayo, Tebello Nyokong*

Department of Chemistry, Rhodes University, P.O. Box 94, Grahamstown 6140, South Africa

ARTICLE INFO

Article history:
Received 29 November 2010
Received in revised form
28 December 2010
Accepted 7 January 2011
Available online 21 January 2011

Keywords:
Photocatalysis
Phthalocyanines
Oxidation
4-Nitrophenol

ABSTRACT

Adsorption of palladium phthalocyanines complexes on single walled carbon nanotubes was carried out. The resulting composites were employed as catalysts for heterogeneous photocatalytic oxidation of 4-nitrophenol (4-NP) in aqueous media. Singlet oxygen was found to be involved in the phototransformation of 4-NP. Gas chromatographic separation gave hydroquinone and benzoquinone as the phototransformation products. Langmuir–Hinshelwood (L–H) model was employed to evaluate the adsorption and desorption equilibria of the reactants and the products. 2,3,9,10,16,17,23,24-octakis(dodecylthiophthalocyaninato) palladium(II) and 1,4,8,11,15,18,22,25-octakis(dodecylthio phthalocyaninato) palladium, containing the longest alkyl chain gave the best performances.

1. Introduction

The toxicity of 4-nitrophenol is well established [1]. The methods which have been investigated for the degradation of 4-nitrophenol (4-NP) include microbial [2] and photocatalytic degradation [3,4]. Photodegradation of 4-NP is preferable since it avoids the use of harsh oxidants. TiO_2, has been found to be an inefficient photosensitiser for degradation of 4-NP due to the fact that its band gap is in the near-UV region where only about 4% of solar energy is effective [5]. Metallophthalocyanine (MPc) complexes have been employed as heterogeneous catalysts for the photodegradation of organic pollutants such as phenols [5]. This is due to their high light absorption capacity in the visible region, photostability, chemical stability and their ability to generate singlet oxygen species, which is implicated in photocatalysis. The supports for phthalocyanines which have been employed for their use in photocatalytic degradation of pollutants, include TiO_2, resins and clays [6–8] with varied degrees of success.

The association of TiO_2 and ZnPc gave a small increase (<6%) in the photodegradation efficiency of phenol compared to TiO_2 alone. This behavior was expected since the light employed had a maximum absorption at 360 nm, where there is insignificant absorption by ZnPc [6], showing the need for visible light excitation of the MPc complexes. In this work we used single walled carbon nanotubes (SWCNTs) as support material for MPc complexes (**1a–1e**, and **2a–c**, Fig. 1). These complexes have been found to show high singlet oxygen quantum yields [9]. Thus, palladium phthalocyanines have potential in the area of photocatalysis because of their singlet oxygen generating ability and photostability [9]. Other common phthalocyanines such as ZnPc derivatives are unstable during photodegradation of 4-NP or other phenols [10,11]. SWCNTs were chosen as support because of ease of immobilisation of MPcs due to the strong π–π interaction between SWCNTs and MPc complexes. Composites of MPc complexes with SWCNTs have been used in electrocatalysis [12–14]. The use of SWCNTs as MPc supports for photocatalysis is reported here for the first time.

The study of the photophysical and photochemical behavior of palladium phthalocyanines (PdPc) is still limited [15–17]. Alkyl thio derivatized phthalocyanine complexes of palladium are scarce, hence in this work we report on the physicochemical behavior of alkylthio and aryloxyl derivatised PdPcs and their use in the phototransformation of 4-NP when adsorbed on SWCNTs.

2. Experimental

2.1. Materials

4-Nitrophenol (4-NP), fumaric acid, benzoquinone, dimethylsulfoxide (DMSO), dichloromethane (DCM), 1-chloronaphthalene (1-CNP), $PdCl_2$, dimethylformamide (DMF) and hydroquinone were purchased from SAARCHEM. Dichloromethane (SAARCHEM) was distilled before use. Octanethiol, dodecanethiol,8-diazabicyclo{5.4.0}-undec-7-ene (DBU), diphenylisobenzofuran (DPBF), anthracene-9,10-bis-methylmalonate (ADMA) and

* Corresponding author. Tel.: +27 46 603 8260; fax: +27 46 622 5109.
E-mail address: t.nyokong@ru.ac.za (T. Nyokong).

1381-1169/$ – see front matter © 2011 Elsevier B.V. All rights reserved.
doi:10.1016/j.molcata.2011.01.016

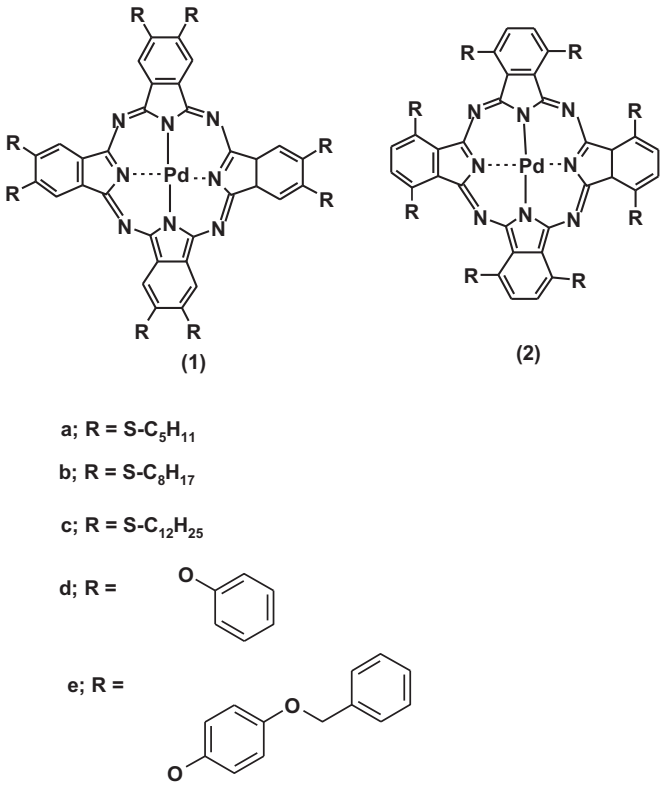

Fig. 1. Molecular structure of the photocatalysts employed in this work.

single wall carbon nanotubes (SWCNTs, 0.7–1.2 nm in diameter and 2–20 μm in length) were from Aldrich. Silica gel 60 (0.063–0.200 mm) was used for column chromatography. Distilled deionised Millipore water was used to prepare aqueous solutions of 4-NP, The syntheses of the following photocatalysts (phthalocyanine complexes): 2,3,9,10,16,17,23,24-octakis(pentylthiophthalocyaninato) palladium(II) (**1a**); 2,3,9,10,16,17,23,24-octakis(octylthiophthalocyaninato) palladium(II) (**1b**); 2,3,9,10,16,17,23,24-octakis(dodecylthiophthalocyaninato) palladium(II) (**1c**); 2,3,9,10,16,17,23,24-octakis(phenoxyphthalocyaninato) palladium (**1d**); 2,3,9,10,16,17,23,24-octakis(benzyloxyphenoxy)phthalocyaninato palladium-(**1e**) and 1,4,8,11,15,18,22,25-octakis(pentylthiophthalocyaninato) palladium (**2a**), Fig. 1, have been reported before [9,18,19]. The syntheses of palladium-1,4,8,11,15,18,22,25-octakis(octylthio)phthalocyanine (**2b**) and palladium-1,4,8,11,15,18,22,25-octakis(dodecylthio)phthalocyanine (**2c**), (hence compounds **4b** and **4c**, Scheme 1) are reported in this work.

2.2. Equipment

X-ray powder diffraction patterns were recorded on a Bruker D8 Discover equipped with a proportional counter, using Cu-Kα radiation (λ = 1.5405 Å, nickel filter). Data were collected in the range from $2\theta = 5^\circ$ to 60°, scanning at 1° min^{-1} with a filter time-constant of 2.5 s per step and a slit width of 6.0 mm. Samples were placed on a silicon wafer slide. The X-ray diffraction data were treated using Eva (evaluation curve fitting) software. Baseline correction was performed on each diffraction pattern by subtracting a spline fitted to the curved background and the full-width at half-maximum values used in this study were obtained from the fitted curves. Samples for transmission electron microscopy (TEM) were prepared by sonnicating the samples of SWCNTs, or ads–MPcs–SWCNT in a mixture of DMF and DCM.

Bruker Vertex 70-Ram II Raman spectrometer (equipped with a 1064 nm Nd:YAG laser and a liquid nitrogen cooled germanium detector) were used to collect Raman data. The Raman spectral data for the SWCNTs, MPcs, ads–MPcs–SWCNT were obtained from their powdered samples. Transmission electron microscope (TEM) pictures were obtained using a JEOL JEM 1210 transmission electron microscope at 100 kV accelerating voltage.

UV–vis spectra were recorded using a Shimadzu UV-2550 UV–vis spectrophotometer. IR data were obtained using the Perkin-Elmer spectrum 2000 FTIR spectrometer. ^{1}H NMR spectra were recorded using a Bruker AMX 400 MHz spectrometer. Elemental analyses were carried out on a Vario EL III MicroCube CHNS Analyzer. The pH of the solutions was measured with Metrohm 827.

Mass spectra data were collected with a Bruker AutoFLEX III Smartbeam TOF/TOF Mass spectrometer. The instrument was operated in positive ion mode using an *m*/*z* range of 400–3000. The voltage of the ion sources were set at 19 and 16.7 kV for ion sources 1 and 2 respectively, while the lens was set at 8.50 kV. The voltages for reflectors 1 and 2 were set at 21 and 9.7 kV respectively. The spectra were acquired using dithranol as the MALDI matrix, using a 354 nm Nd:YAG laser.

Photoirradiation experiments for singlet oxygen quantum yields and phototransformation of 4-nitrophenol were carried out using a tungsten lamp (100 W, 30 V). A 600 nm glass cut off filter (Schott) and a water filter were used to filter off ultraviolet and infrared radiations, respectively. Light intensities were measured with a POWER MAX5100 (Mol-electron detector incorporated) power meter. For singlet oxygen quantum yield determinations for complexes **2a–2c**

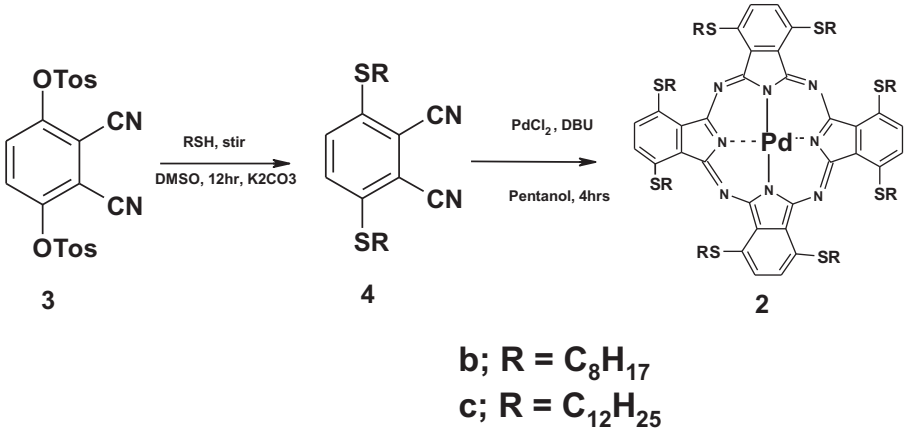

Scheme 1. The syntheses of palladium-1,4,8,11,15,18,22,25-octakis(alkylthio)phthalocyanine.

in 1-CNP, an interference filter (Intor, 750 nm with a band width of 40 nm) was additionally placed in the light path before the sample, to ensure the excitation of the Q band. For the determination of singlet oxygen quantum yields of ads–MPc–SWCNT conjugates, interference filters of 670 nm (for **1a–1e**) and 750 nm (for **2a–2c**) were employed.

Triplet quantum yields and lifetimes of the new complexes (**2a–2c**) were determined using a laser flash photolysis system; the excitation pulses were produced by a Nd:YAG laser (Quanta-Ray, 1.5 J/8 ns) pumping a dye laser (Lambda Physic FL 3002, Pyridin 1 in methanol). The analyzing beam source was from a Thermo Oriel xenon arc lamp, and a photomultiplier tube was used as a detector. Signals were recorded with a two-channel digital real-time oscilloscope (Tektronix TDS 360); the kinetic curves were averaged over 256 laser pulses. Triplet lifetimes were determined by exponential fitting of the kinetic curves using Origin Pro 7.5 software.

2.3. Photocatalysis procedures

The singlet oxygen quantum yield (Φ_Δ) determinations (for the new complexes **2a–2c**) were carried out using 1-CNP solutions containing DPBF (90 μM) and the Pcs (absorbance ~ 0.2 at the irradiation wavelength). Irradiations were done using the set-up described above, and were repeated until around 80% decay of DPBF was observed [20]. The absorbance was corrected for that of the sensitizer in the B band region. Singlet oxygen quantum yields of the ads–MPc–SWCNT conjugates were determined by suspending the conjugates in oxygen saturated pH 8.5 buffer solution and irradiating at the Q band of the phthalocyanine complexes, using ADMA as a singlet oxygen quencher in aqueous media.

The transformation of 4-NP was monitored through its absorption peak at 400 nm after each photolysis cycle. A 1 cm path-length UV–vis spectrophotometric cell, fitted with a tight fitting stopper was used as the reaction vessel. The pH of the 4-NP solution was adjusted to 8.5. At this pH, 4-NP is deprotonated. The participation of $^1O_2$ in the photolysis of 4-NP was further confirmed by the addition of sodium azide, a singlet oxygen quencher, to the photolysis reaction containing the 4-NP and suspended ads–MPc–SWCNT.

The photocatalysis products were analysed using gas chromatography (GC). For the GC analysis, Agilent Technologies 6820 GC system (HP 5973, HP-1 column) was employed. The photolysed solutions were filtered to remove the MPc-SWCNT particles before GC analysis.

2.4. Triplet and singlet oxygen quantum yield parameters

Triplet quantum yields were determined using a comparative method based on triplet decay, using Eq. (1):

$$\Phi_T^{Sample} = \Phi_T^{Std} \frac{\Delta A_T^{Sample} \varepsilon_T^{Std}}{\Delta A_T^{Std} \varepsilon_T^{Sample}} \quad (1)$$

where ΔA_T^{Sample} and ΔA_T^{Std} are the changes in the triplet state absorbance of the PdPc derivatives and the standard, respectively. ε_T^{Sample} and ε_T^{Std} are the triplet state extinction coefficients for the PdPc derivatives (**2a–c**) and standard, respectively. Φ_T^{Std} is the triplet state quantum yield for the standard, ZnPc in 1-CNP, $\Phi_T^{Std} = 0.67$ [21]. Triplet lifetimes were determined by exponential fitting of the kinetic curves using OriginPro 7.5 software.

The DPBF (or ADMA) quantum yields (Φ_{DPBF}) were calculated using Eq. (2) and the determined extinction coefficient of DPBF in 1-chloronaphthalene ($\varepsilon_{1\text{-CNP}} = 20287\ M\ L^{-1}\ cm^{-1}$).

$$\Phi_{DPBF} = \frac{(C_0 - C_t)V_R}{I_{abs} t} \quad (2)$$

where C_0 and C_t are the DPBF concentrations prior to and after irradiation, respectively; V_R is the reaction volume; t is the irradiation time per cycle and I_{abs} is defined by Eq. (3).

$$I_{abs} = \frac{\alpha A I}{N_A} \quad (3)$$

where $\alpha = 1 - 10^{-A(\lambda)}$, $A(\lambda)$ is the absorbance of the sensitizer at the irradiation wavelength, A is the irradiated area (3.14 cm^2), I is the intensity of light (1×10^{15} photons $cm^{-2}\ s^{-1}$) and N_A is Avogadro's constant. The singlet oxygen quantum yields (Φ_Δ) were calculated using Eq. (4).

$$\frac{1}{\Phi_{DPBF}} = \frac{1}{\Phi_\Delta} + \frac{1}{\Phi_\Delta}\frac{k_d}{k_a}\frac{1}{[DPBF]} \quad (4)$$

where k_d is the decay constant of singlet oxygen and k_a is the rate constant for the reaction of DPBF with $O_2(^1\Delta_g)$. The value of $1/\Phi_\Delta$ for the PdPc derivatives **2a–2c** was obtained as the intercept from the plot of $1/\Phi_{DPBF}$ versus 1/DPBF. The singlet oxygen quantum yields of ads–MPc–SWCNT conjugates were calculated as described above, using ADMA as singlet oxygen quencher and substituting it for DPBF.

2.5. Synthesis of complexes *2b* and *2c*

Synthesis of **1a–e** and **2a** (hence **4a**) have been reported [9,18,19]. Synthesis of compound **3** has also been reported [22], Scheme 1.

2.5.1. 3,6-Di(octylthiol)-4,5-dicyanobenzene (*4b*)

Following literature methods for synthesis of substituted phthalonitriles [20], **4b** was synthesized as follows: octanethiol (2.01 g, 20 mmol) was dissolved in dimethylsulfoxide (DMSO) (15 ml) under nitrogen and **3** (2 g, 10 mmol) was added. After stirring for 15 min, finely ground anhydrous potassium carbonate (6 g, 43.4 mmol) was added portion-wise within 2 h with efficient stirring. The reaction mixture was stirred under nitrogen at room temperature for 12 h. Then water (30 ml) was added and the aqueous phase extracted with chloroform (3× 20 ml). The combined extracts were treated first with sodium carbonate solution (5%), followed by water. The solvent was evaporated and the product was crystallized from ethanol. Yield: 2.4 g (79%). ^{1}H NMR (400 mHz); δ ppm ($CDCl_3$) 7.52 (2H, s, Ar–H), 3.06–3.02 (4H, t, $-CH_2$), 1.74–1.68 (4H, m, $-CH_2$), 1.48–1.45 (4H, m, $-CH_2$), 1.31–1.29, (16H, m, $-(CH_2)_4$), 0.93–0.90 (6H, m, $-CH_3$). IR (KBr pellets) ν_{max}/cm^{-1}]: 3469, 3094, 3021, 2934, 2871, 2574, 2232(C≡N), 1827, 1573, 1469, 1226, 1127, 916, 734(C–S), 687, 539.

2.5.2. 3,6-Di(dodecylthiol)-4,5-dicyanobenzene (*4c*)

The same method used for the synthesis of **4b** was also used for **4c** except dodecylthiol was employed instead of octanethiol. The amounts of reagents used were: dodecanethiol (3.01 g, 20 mmol), 3 (2 g, 10 mmol), potassium carbonate (6 g, 43.4 mmol). Yield: 4.4 g (85%). ^{1}H NMR (400 mHz); δ ppm ($CDCl_3$): 7.52 (2H, s, Ar–H), 3.04–3.01 (4H, t, $-CH_2$), 2.71–2.68 (4H, m, $-CH_2$), 1.70–1.66, (12H, m, $-(CH_2)_3$), 1.29–1.24, (12H, m, $-(CH_2)_3$), 0.93–0.90 (18H, m, $-(CH_2)_3-CH_3$). IR (KBr pellets) ν_{max}/cm^{-1}]: 3468, 3090, 3024, 2931, 2868, 2577, 2231(C≡N), 1822, 1579, 1462, 1353, 1129, 921, 741(C–S), 683.

2.5.3. 1,4,8,11,15,18,22,25-Octakis(octylthiophthalocyaninato) palladium(II) (*2b*)

In refluxing pentanol (10 ml), 3,6-bis(octylthio)-4,5-dicyanobenzene (**4b**) (0.42 g, 1 mmol), $PdCl_2$ (0.08 g, 0.45 mmol) and DBU (1.70 g, 11.17 mmol) were added. The solution was heated to reflux for 5 h. The solution was then allowed to cool and the solvent removed under reduced pressure, followed by

titration with cold methanol to precipitate the product. The black precipitate was dissolved in DCM and passed through a silica column, DCM was used as the eluting solvent to afford **2b**. Yield: 0.22 g (56%). UV/vis [(1-chloronaphthalene/λ_{max}/nm (log ε)] 756 (4.6), 679 (4.25). $C_{96}H_{144}N_8PdS_8$: Cald.: C, 59.34; H, 7.40; N, 5.70%; Found, C, 59.02; H, 8.01; N,5.12%. ^{1}H NMR (400 MHz, $CDCl_3$) δ_H/ppm: 8.22 (8H, s, Ar–H), 3.40 (16H, m, S–CH_2), 1.61–1.31 (120H, m, –$(CH_2)_6$–CH_3)); Calc. MS (ESI–MS) *m/z*: Calc. 1773.16; Found $[M]^+$: 1772.22 [IR (KBr pellets) ν_{max}/cm^{-1}]: 2962, 2930, 2858, 1466, 1414, 1381, 1264, 1143, 1078, 969, 874, 747(C–S).

2.5.4. 1,4,8,11,15,18,22,25-Octkis(dodecylthiophthalocyaninato) palladium(II) (*2c*)

The same method used for **2b** was employed for the synthesis of **2c**, except that **4c** instead of **4b** was employed. The amounts of the reagents were the same. Yield: 0.28 g (53%). UV/vis [(1-chloronaphthalene/λ_{max}/nm (log ε)] 756 (4.71), 679 (4.28). $C_{130}H_{212}N_8PdS_8$: Cald.: C, 64.43; H, 8.70; N, 4.60%. Found, C, 63.94; H, 8.51; N, 4.19%; ^{1}H NMR (400 MHz, $CDCl_3$) δ_H/ppm: 8.32 (8H, s, Ar–H), 3.41 (16H, m, S–CH_2), 1.22–0.77 (184H, m, –$(CH_2)_{10}$–CH_3)); Calc. MS (ESI–MS) *m/z*: Calc. 2251.07; Found $[M]^+$: 2250.12 [IR (KBr pellets) ν_{max}/cm^{-1}]: 2929, 2858, 1729, 1472, 1377, 1269, 1108, 998, 818, 751 (C–S), 647.

2.6. Purification and functionalisation of SWCNTs

SWCNTs were purified (by oxidation) to form SWCNT–COOH by adding raw SWCNTs (100 mg) to a mixture of concentrated HNO_3 and concentrated H_2SO_4 (3:1) [23] The resulting suspension was stirred at a temperature of 70 °C for 2 h. The final mixture was cooled to room temperature and washed with excess millipore water until a pH of 5 was obtained. The purified SWCNTs (SWCNT–COOH) were dried in an oven for 12 h.

2.7. Immobilisation of MPcs on SWCNTs

Each of the PdPc derivatives was dissolved in DCM to give an absorbance of approximately 2. Purified SWCNTs (50 mg) were added to each of the PdPc solutions. The mixture was stirred until there was no change in absorbance of the MPcs. The mixture was then centrifuged and the supernatant was decanted, leaving the particles of MPcs adsorbed on SWCNTs (represented as ads–MPc–SWCNT). The particles were washed with distilled deionised water, methanol and acetone, followed by air drying for 24 h. The concentration of MPcs adsorbed was calculated from the differences in absorbances to be 1.0×10^{-8} M.

3. Results and discussions

3.1. Characterization of complexes *2a–2c*

Synthesis of **2a** has been reported [19], but the photophysical and photochemical properties are reported in this work.

Complexes **2b** and **2c** were synthesized by treating the corresponding phthalonitriles (**4b** and **4c**) with palladium chloride in 1-pentanol using DBU as catalyst, Scheme 1. Column chromatography with silica gel was employed to obtain the pure products. The MPc derivatives were characterized by UV–vis, mass, IR and NMR spectroscopies, and elemental analyses. The sharp peak for the C≡N vibrations in the IR spectra of phthalonitriles at 2231 (**4c**) and 2232 cm^{-1} (**4b**) disappeared after conversion into phthalocyanines. The phthalocyanines showed vibrations due to C–S–C group between 751 and 747 cm^{-1}. Mass and proton NMR spectral data as well as elemental analysis were additionally employed to characterize the complexes, and the data are consistent with the structures of the complexes. The elemental analyses results gave

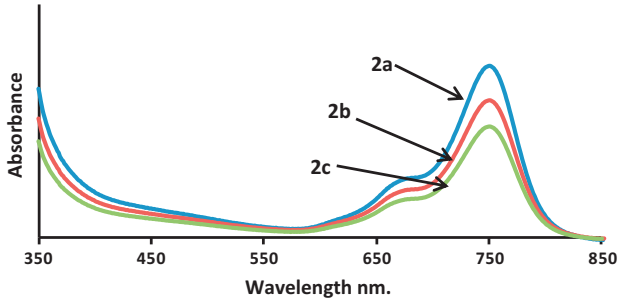

Fig. 2. UV–vis spectra of complexes **2a–2c** in 1-CNP. Concentration ~1×10^{-5} M.

Table 1
Spectroscopic, photophysical and photochemical data for complexes **2a–2c** in 1-CNP.

Complex	Q band maxima	Φ_Δ	Φ_T	τ_T (μs)
2a	756	0.39	0.42	13
2b	756	0.37	0.41	11
2c	756	0.37	0.39	8

percentage carbon values that were within 1% in all cases, which are within acceptable range for phthalocyanine complexes [24].

Fig. 2 shows the ground state electronic absorption spectra of compounds **2a–2c** in 1-CNP. The Q band maxima were observed at 756 nm (Table 1). These values were 745 nm in DCM. The complexes were not aggregated in 1-CNP, and Beer–Lambert law was obeyed for concentration below 1×10^{-5} M.

Fig. 3a shows the transient absorption spectrum of complex **2c** in 1-CNP and Fig. 3b shows the triplet decay curve for **2c** in 1-CNP. The triplet absorption was observed at 580 nm, Fig. 3a (insert). The triplet quantum yields (Φ_T) for **2a**, **2b** and **2c** were 0.42, 0.41

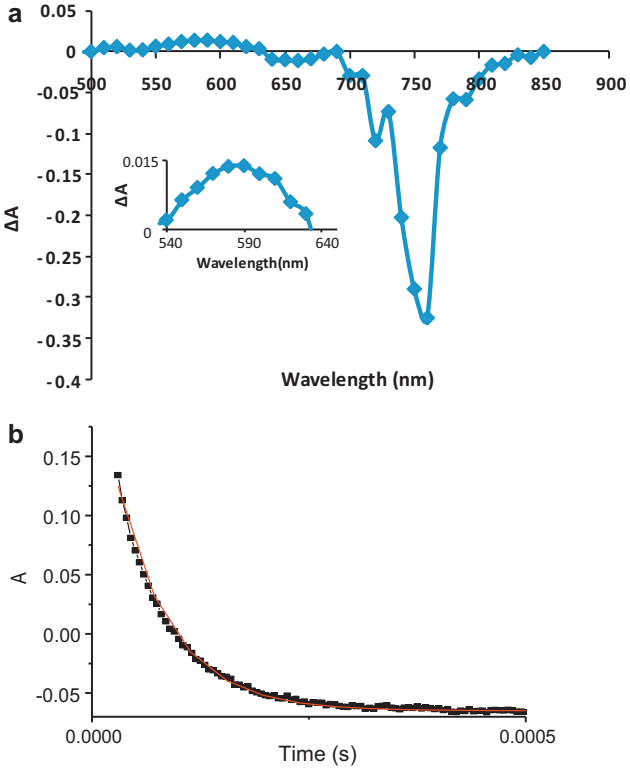

Fig. 3. (a) Transient absorption spectrum of complex **2c** in 1-CNP. Inset = triplet state absorption maximum. (b) Triplet decay curve of **2c** in 1-CNP at 590 nm. Excitation wavelength = 750 nm.

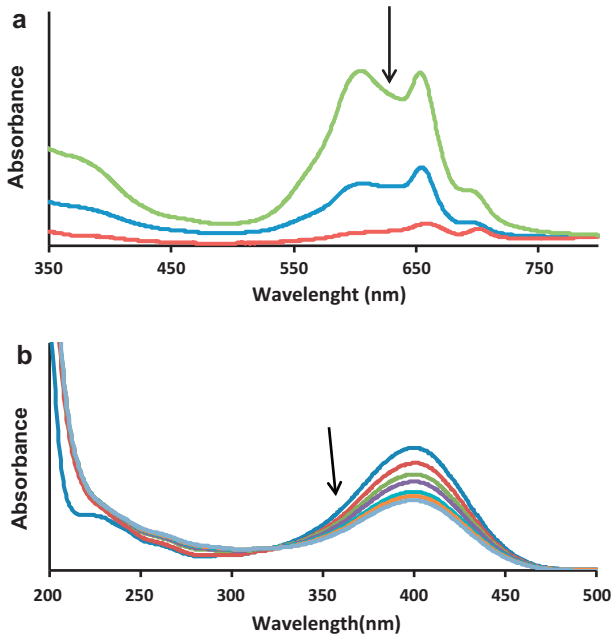

Fig. 4. Spectral changes showing (a) the disappearance of complex **1a** during its immobilization on SWCNT–COOH (200 mg). Initial concentration of **1a** = 1.2×10^{-5} mol dm^{-3}; time = 50 min) and (b) adsorption of 4-NP on SWCNTs (in the absence of MPc complexes).

and 0.39, respectively in 1-CNP (Table 1). These values are similar to those of complexes **1a–d** reported before, which ranged from 0.40 to 0.51, with the exception of **1e** which gave a large value of $\Phi_T = 0.65$ [9]. The triplet lifetimes (τ_T) were 13 μs (**2a**), 11 μs (**2b**) and 8 μs (**2c**), and are also similar to those reported for **1a–1e**. The low values of τ_T were expected due to the open-shell nature of the Pd central metal. The singlet oxygen quantum yields (Φ_Δ) were 0.39 (**2a**), 0.37 (**2b**) and 0.37 (**2c**) in 1-CNP. The reported values for **1a–1e** ranged between 0.39 and 0.49 in 1-CNP [9,18].

3.2. UV–vis spectral studies of the immobilisation of MPcs on SWCNTs to form ads–MPc–SWCNT

Immobilization of PdPc complexes on SWCNTs was carried out by stirring DCM solutions of the PdPc derivatives in the presence of SWCNTs until there was no change in absorbance of the former, this was done over a period of 5 h or more depending on the PdPc derivative. The changes in absorbance of solution of complex **1a** in DCM over time during stirring in the presence of SWCNTs are shown in Fig. 4a. The spectrum of complex **1a** shows extensive aggregation in DCM as has been reported before [18]. Aggregation is judged by the presence of a broad band near 600 nm due to the aggregate and a sharper one at 650 nm, due to the monomer. Aggregation was displayed by all complexes. The small peak at 690 nm has been explained in previous study [18] as being due to intermolecular interaction between the central metal ion of one molecule with the thio group of another. On addition of SWCNTs to solution of **1a**, followed by stirring, there was a decrease in absorbance of complex **1a** as it adsorbs onto SWCNTs, Fig. 4a. The resulting conjugate is represented as ads–MPc–SWCNT–COOH. The peak at 690 nm however persists during immobilization suggesting that the interactions are still present.

SWCNTs are known to directly adsorb phenols [25,26] as shown in Fig. 4b. In order to check if following immobilization of PdPc derivatives onto SWCNTs, there were still parts of SWCNTs which were exposed, experiments were carried out where ads–MPc–SWCNT–COOH was immersed in a solution of 4-NP without photolysis. There was a slight decrease in the absorbance of

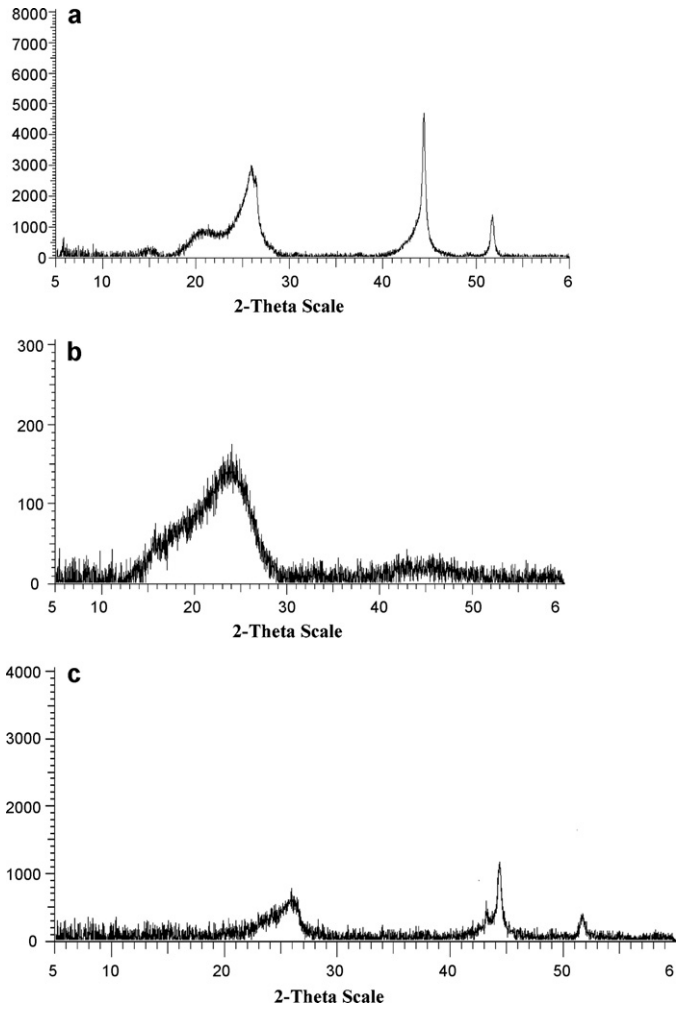

Fig. 5. XRD spectra of (a) SWCNT–COOH, (b) complex **1c** and (c) ads–**1c**–SWCNT–COOH.

4-NP (an average of 5%), showing that some empty sites were still left on SWCNTs where 4-NP could adsorb. The final spectrum following the adsorption of 4-NP (before photolysis) was used as the starting spectrum for all calculations done in this work. Experiments were also performed where PdPc derivatives were suspended in a solution of 4-NP without photolysis, and there were no changes in spectra confirming that the latter does not adsorb on the former. Experiments were also performed where SWCNTs following adsorption of 4-NP was photolysed in pH 8.5 buffer only. There were no changes in absorbance which could be attributed to leaching of 4-NP (or its oxidation products) from the SWCNTs.

3.3. Characterization ads–MPc–SWCNT

3.3.1. XRD

X-ray diffraction technique was used to confirm the formation of SWCNT-MPc composites. Variations in nature and positions of peaks on XRD spectra are reflective of changes in structural features of the sample under consideration. Fig. 5 shows the XRD spectra of SWCNT–COOH, complex **1c** alone and ads–**1c**–SWCNT–COOH. Fig. 5a (for SWCNT–COOH) shows sharp ($2\theta = 44.5^\circ$ and 51.9°) and broad ($2\theta = 29.4^\circ$ and 25.9°) peaks that are indicative of the crystalline and amorphous natures of the SWCNT–COOH, respectively. Using international centre for diffraction data (ICDD) database, the peak at $2\theta = 25.9^\circ$ are ascribed to (0 0 2) *d*-spacing of the SWCNT–COOH [27,28], while peaks at $2\theta = 44.4^\circ$ and 51.9° are char-

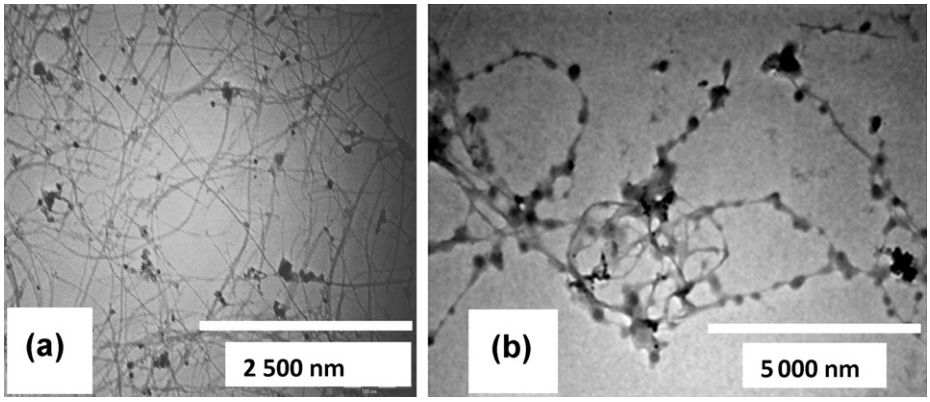

Fig. 6. TEM images of (a) SWCNTs (magnification 10,000×) and (b) ads–**1c**–SWCNT (magnification 20,000×).

acteristic of (1 0 0) [27], and (2 0 0) [28] reflections of carbon of the SWCNT–COOH, respectively. The only prominent peak in the XRD spectrum of complex **1c** was a broad one at $2\theta = 24.1^\circ$ (Fig. 5b). Its broadness is an indication of the amorphous nature of complex **1c**. In the XRD spectrum ads–**1c**–SWCNT–COOH (Fig. 5c), the peak near 25° encompasses both **1c** and SWCNT–COOH. The differences in spectra indirectly suggest the presence of a conjugate of SWCNTs and **1c**.

3.3.2. Raman spectroscopy

Raman spectroscopy is used for the characterization of disordered polycrystalline graphitic carbons. The Raman spectra of graphite show a pair of bands at about 1360 and at 1560 cm^{-1}. These two bands are the most diagnostic features, and are designated as D and G bands, respectively. Raman spectroscopy can be used to some extent to quantify changes in the SWCNTs using the ratio of D/G bands under fixed laser power intensity.

Adsorption of MPc complexes may not cause extensive disruption to the carbon lattice due to the non-invasive π-π interactions i.e. preservation of the carbon nanotube structure, however small changes in the D/G ratio may indicate the presence of MPcs on the SWCNTs skeleton. We observed the G band at 1593 cm^{-1} for SWCNT–COOH and the D band at 1382 cm^{-1}, which shifted to 1490 cm^{-1} for ads–MPc–SWCNT (figures not shown). Functionalization of SWCNTs is known to enhance the D band [29–31] hence the increase in the D/G ratio from 0.47 for SWCNT–COOH to 0.85 for ads–MPc–SWCNT, indirectly confirms adsorption of PdPc derivatives on SWCNT–COOH.

3.3.3. Transmission electron microscopic (TEM) characterization

TEM technique provided a microscopic view of the ads–MPc–SWCNT–COOH. Fig. 6a is the TEM image of SWCNT–COOH. The image obtained after the formation of the adsorbed specie, ads–**1c**–SWCNT–COOH (Fig. 6b) was completely different showing coverage of the large portion of the surface of SWCNTs with PdPc derivatives.

3.4. Singlet oxygen generation capacity of ads–MPc–SWCNT in pH 9 buffer

Since singlet oxygen is thought to be involved in the photocatalysis mechanism, its generation by ads–MPc–SWCNT was investigated. As stated in the experimental, different interference filters were employed for peripheral (**1a–1e**) and non-peripheral **2a–2c**, to ensure excitation of the low energy peak due to the monomer of the adsorbed Pc. This assumes that Q band maxima of the absorbed specie are about the same as that in solution with the expected broadening in the former. An aqueous solution of 6.0×10^{-5} mol dm^{-3} ADMA containing a suspension of each of the ads–MPc–SWCNT conjugates, was successively irradiated at the Q-band of MPc, centrifuged and decanted into UV–vis cell and absorbance recorded. The change in absorbance of ADMA at 379 nm (Fig. 7) shows that singlet oxygen is formed on photolysis of ads–MPc–SWCNT in the presence of ADMA. The spectra of the MPcs were not observed since they acted as heterogenous catalysts in the reactions. The rather low Φ_Δ values of ads–MPc–SWCNT (0.19–0.27, Table 2) under heterogenous condition compared with what was obtained in solution [9] are ascribed to inefficient energy transfer to ground state oxygen or the solid nature of the molecules (in the former) which might encourage more aggregation.

3.5. Photocatalytic behavior of ads–MPc–SWCNT towards 4-NP

UV–vis spectroscopy was employed to monitor the transformation of 4-NP. Since the pK_a of 4-nitrophenol is 7.15 these studies were carried out in aqueous solution at pH 8.5 because phenolate ions which are more oxidizable are predominant at these conditions. It is important to state that no change in spectra of 4-nitrophenol was observed when photolysis was done in the absence of ads–MPc–SWCNT. Also no transformation was observed when 4-nitrophenol was stirred in the presence of ads–MPc–SWCNT without photolysis. During photolysis at the Q band region of the PdPc derivatives, in the presence of suspended ads–MPc–SWCNT (Fig. 8a), there was a gradual collapse of the 4-NP peaks at 250 and 400 nm. There was also an increase in the absorbance near 220 nm, possibly due to the photolysis products, however, absorption in this region will be affected by solvents. It is important to note that the

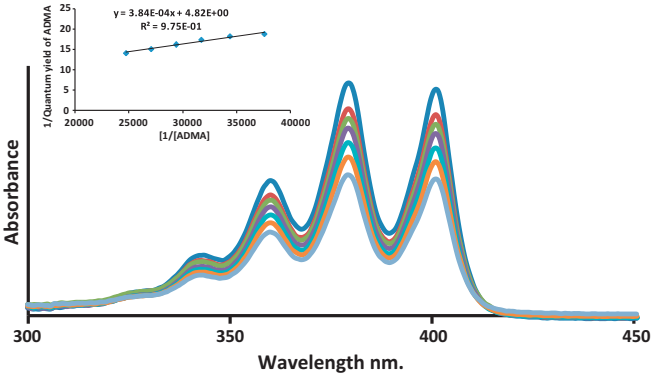

Fig. 7. Electronic absorption spectral changes observed during the photolysis of (a) ADMA to confirm singlet oxygen production by ads–**2c**–SWCNT. Initial ADMA concentration = 6.0×10^{-5} mol dm^{-3}; time = 60 min. Inset: plot of $1/\Phi_{ADMA}$ versus 1/[ADMA] for the determination of singlet oxygen quantum yield using Eq. (4).

Table 2
Langmuir–Hinshelwood (L–H) parameters for the phototransformation of 4-NP on ads–MPc–SWCNT and singlet quantum yields of the complexes (in the presence of SWCNTs) at pH 8.5.

Complex	4-NP (M)	k_{obs} ($\times 10^{-3}$ min^{-1})	Φ_Δ	k_r ($\times 10^{-6}$ M min^{-1})	K_{ads} ($\times 10^{3}$ M^{-1})
Ads–**1a**–SWCNT	4.00×10^{-5}	3.00	0.22	1.3	0.51
	6.00×10^{-5}	2.25			
	8.00×10^{-5}	1.52			
	1.00×10^{-4}	0.61			
1b	4.00×10^{-5}	2.7	0.22	1.1	0.42
	6.00×10^{-5}	2.1			
	8.00×10^{-5}	1.32			
	1.00×10^{-4}	0.42			
1c	4.00×10^{-5}	3.16	0.27	1.8	3.8
	6.00×10^{-5}	2.40			
	8.00×10^{-5}	1.74			
	1.00×10^{-4}	0.75			
1d	4.00×10^{-5}	2.22	0.19	0.7	0.19
	6.00×10^{-5}	1.64			
	8.00×10^{-5}	0.92			
	1.00×10^{-4}	0.11			
1e	4.00×10^{-5}	2.51	0.20	1.0	0.37
	6.00×10^{-5}	1.95			
	8.00×10^{-5}	1.27			
	1.00×10^{-4}	0.32			
2a	4.00×10^{-5}	3.19	0.23	1.4	0.33
	6.00×10^{-5}	2.27			
	8.00×10^{-5}	1.67			
	1.00×10^{-4}	0.63			
2b	4.00×10^{-5}	2.79	0.21	1.3	0.32
	6.00×10^{-5}	2.41			
	8.00×10^{-5}	1.33			
	1.00×10^{-4}	0.54			
2c	4.00×10^{-5}	3.29	0.20	1.9	2.8
	6.00×10^{-5}	2.67			
	8.00×10^{-5}	1.86			
	1.00×10^{-4}	0.98			

spectra in Fig. 8a were recorded after allowing the initial adsorption of small amounts of 4-NP onto SWCNTs (without photolysis), until no change in electronic absorption spectra of 4-NP was observed. The spectral changes shown in Fig. 8a were also observed for SWCNTs composite of complexes **1b**, **1c**, **1d**, **1e**, **2a**, **2b** and **2c** though the rate of decrease in the 4-NP varied significantly.

3.6. Kinetic studies for photolysis of 4-NP

As shown in Fig. 8b the kinetics of transformation of 4-nitrophenol fitted into pseudo first order reaction kinetics. The apparent rate constant k_{obs} was obtained from the slopes in Fig. 8b for all the MPcs composites for different concentrations of 4-nitrophenol ranging from 4×10^{-5} to 10×10^{-5} M. The apparent rate of reaction (k_{obs}) for all ads–MPc–SWCNT in Table 2, show that the more dilute the 4-NP solution, the higher the apparent rate for transformation. The k_{obs} values ranged from 6.10×10^{-4} min^{-1} to 3.00×10^{-3} min^{-1} (ads–**1a**–SWCNT), 4.20×10^{-4} min^{-1} to 2.70×10^{-3} min^{-1} (ads–**1b**–SWCNT), 7.50×10^{-4} min^{-1} to 3.16×10^{-3} min^{-1} (ads–**1c**–SWCNT), 1.10×10^{-4} min^{-1} to 2.22×10^{-3} min^{-1} (ads–**1d**–SWCNT), 3.20×10^{-4} min^{-1} to 2.51×10^{-3} min^{-1} (ads–**1e**–SWCNT), 6.30×10^{-4} min^{-1} to 3.19×10^{-3} min^{-1} (ads–**2a**–SWCNT), 5.40×10^{-4} min^{-1} and 2.79×10^{-3} min^{-1} (ads–**2b**–SWCNT) and 9.80×10^{-4} min^{-1} to 3.29×10^{-3} min^{-1}(ads–**2c**–SWCNT) for 4-NP concentrations of 4, 6, 8 and 10×10^{-5} M.

It is important to establish if the transformation reaction takes place following adsorption and to determine the adsorption coefficients. Langmuir–Hinshelwood model was employed for these studies.

Langmuir–Hinshelwood (L–H) equation (Eq. (5)) has been used to describe the competitive adsorption of substrates, reaction intermediates and phenolic oxidant products [32,33].

$$\frac{1}{\text{rate}} = \frac{1}{K_r} + \frac{1}{K_r K_{ads} C_0} \quad (5)$$

where k_r is the rate constant for the adsorption of 4-NP, C_0 is the initial concentration of the substrate (in this case 4-NP). K_{ads} is the adsorption coefficient and represents the equilibrium between the rates of adsorption and desorption [34]. The adsorption studies here are for 4-NP (or intermediates) on PdPc derivatives.

The plots of reciprocal of initial rate of phototransformation (after 60 min of irradiation) versus reciprocal of initial concentration of 4-NP (Fig. 8c) gives k_r as the intercept, the adsorption coefficient (K_{ads}) can now be determined from the slope. For the MPc-SWCNT composites of **1a–1e**, **2a–2c**, the plots were found to be linear with a non-zero intercept. The values of k_r and K_{ads} are shown in Table 2. According to Table 2, adsorption rate (k_r) was the lowest for ads–**1d**–SWCNT where **1d** is substituted with benzyl groups and ads–**1c**–SWCNT and ads–**2c**–SWCNT where complexes **1c** and **2c** contain the longest alkyl chain, gave the largest k_r values, Table 2. Thus the adsorption rate of 4-NP is highest for long chain alkyl phthalocyanines on SWCNTs than for aryl group substituted phthalocyanines. Also for ads–**1c**–SWCNT and ads–**2c**–SWCNT adsorption of 4-NP (or its phototransformation products) is more favoured over desorption compared to the rest of the complexes.

3.7. Catalyst stability

Following use for the photogegradation of 4-NP, the ads–MPc–SWCNT were cleaned by rinsing in water, dried and reused for the phototransformation of 4-NP. Fig. 9 shows the plots of concentration versus time, for the first, second and third uses of ads–**1c**–SWCNT for the phototransformation of fresh

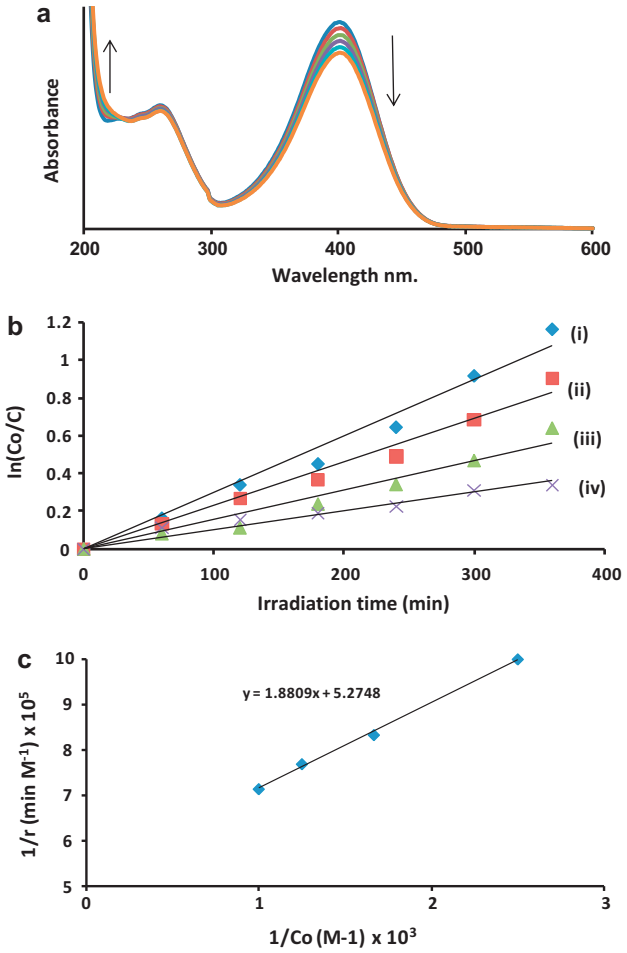

Fig. 8. (a) Spectral changes observed during photolysis of 4-NP using ads–**1a**–SWCNT–COOH. Initial 4-NP concentration = 1.00×10^{-4} mol dm^{-3}. (b) Plot of change in concentration with time during photolysis of 4-NP for different starting 4-NP concentrations using ads–**1c**–SWCNT–COOH as a photocatalyst ((i) 4×10^{-5}, (ii) 6×10^{-5}, (iii) 8×10^{-5} and (iv) $=10 \times 10^{-5}$ M), and (c) Langmuir–Hinshelwood kinetic plot for ads–**2c**–SWCNT–COOH in basic media.

solution of 4-NP. The rates changed from 1.21×10^{-6} M min^{-1} for the first use to 1.11×10^{-6} M min^{-1} for the second use and to 1.04×10^{-6} M min^{-1} for the third use. The rate decreased gradually by ~7% with each run beyond the three runs shown in Fig. 9. The gradual reduction in rate might be due to permanent adsorption of intermediates on the surface of the catalysts thereby reducing their activities or due to degradation of the PdPc catalysts. TEM, XRD and Raman showed that the catalysts were still intact on the surface of the SWCNTs, since there were no changes in the images or spectra following the first uses. Compared to ZnPc derivatives

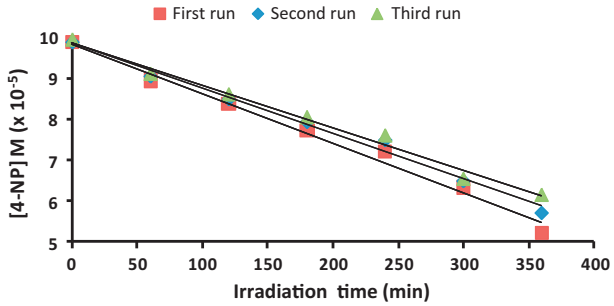

Fig. 9. Plots of concentration versus time for the reuse of ads–**1c**–SWCNT–COOH for the phototransformation of 4-nitrophenol. pH 9 buffer.

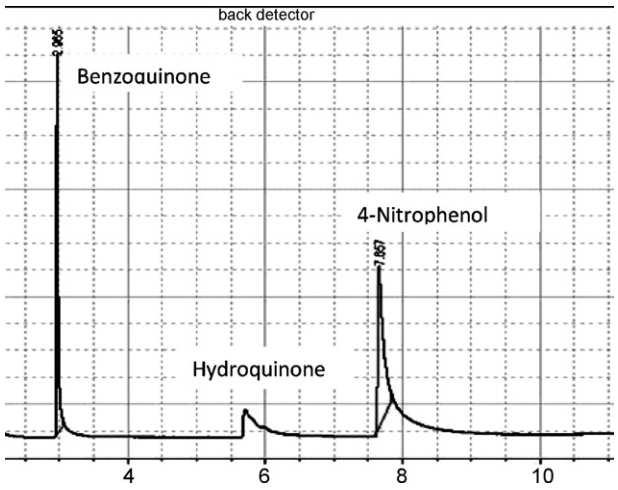

Fig. 10. Gas chromatogram of the photolysed 4-NP sample by ads–**1c**–SWCNT–COOH. Irradiation time = 24 h, starting 4-NP concentration = 1×10^{-4} mol dm^{-3}.

where decreases in stabilities by 15–20% have been reported [10], the present PdPc catalyst shows improved stability.

3.8. Mechansim of 4-NP phototransformation

GC was used to determine the nature of the products of phototransformation reaction by comparing the retention times of expected standards for the catalyzed phototransformation of 4-nitrophenol. These include fumaric acid, 4-nitrocatechol, 1,4-benzoquinone and hydroquinone. Two new peaks which were observed on the gas chromatogram traces, Fig. 10, after irradiation for 24 h. These were identified (using spiking with standards) as hydroquinone and 1,4-benzoquinone. According to the chromatograms hydroquinone was present in a small quantity while the major product was benzoquinone, which was the final product, The contribution of singlet oxygen in the phototransformation process was determined by using ads–**1c**–SWCNT in the presence of a singlet oxygen scavenger, sodium azide. The rate of the reaction was much slower in the presence of NaN_3, Fig. 11, meaning that the reaction proceeded through mainly Type II mechanisms, Scheme 2. When the reaction medium was deareated the two products were still present but benzoquinone appeared to be in smaller quantities than in air, suggesting possible involvement of Type I (radical) mechanism, giving mainly hydroquinone while Type II (singlet oxygen) mechanism gives mainly benzoquinone. The production of benzoquinone is likely from the direct oxidation of 4-NP by singlet oxygen as observed for 4-chlorophenol [35]. The products obtained

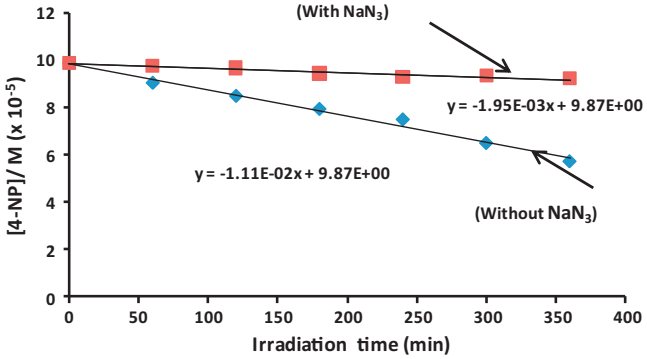

Fig. 11. Demonstration of the effect of sodium azide on 4-NP photo transformation rate using ads–**1c**–SWCNT–COOH.

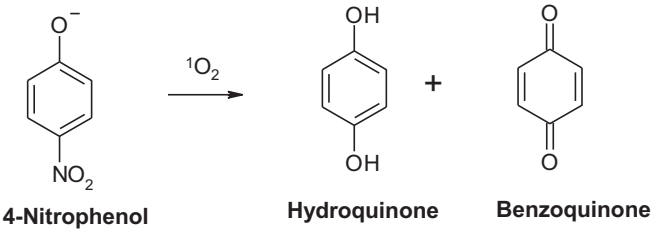

Scheme 2. Proposed mechanism for the phototransformation of 4-NP on ads–MPc–SWCNT–COOH.

are similar to those obtained (as intermediates) in the past work for heterogenous photo-oxidation of 4-nitrophenol [36]. Fumaric acid and 4-nitrocatechol were also observed as final products for ZnPc derivatives suspended in solution [36]. However, the use of SWCNT as supports has advantages of ease of immobilization of MPcs and ease of removal from solution. Preliminary studies on transformation of other phenols (pentachlorophenol) using PdPc complexes immobilized on SWCNT show faster rates of phototransformation.

4. Conclusions

This work demonstrates that the complexes investigated are capable of adsorption onto single wall carbon nanotubes (SWCNTs) forming conjugates. These conjugates were employed for the photooxidation of 4-nitrophenol. Adsorbed β-palladium octakis(dodecylthio)phthalocyanine (**1c**) and α-palladium octakis(dodecylthio)phthalocyanine (**2c**) gave the best performance in terms of adsorption rate of 4-NP. Hydroquinone and benzoquinone were observed as the phototransformation products of 4-NP.

Acknowledgements

This work was supported by the Department of Science and Technology (DST) and National Research Foundation (NRF) of South Africa through DST/NRF South African Research Chairs Initiative for Professor of Medicinal Chemistry and Nanotechnology and Rhodes University. T.O. thanks African Laser centre for graduate bursary.

References

[1] F.J. Zieris, D. Feind, W. Huber, Arch. Environ. Contam. 17 (1988) 165–175.
[2] S. Laha, K.P. Petrova, Biodegradation 8 (1998) 349–356.
[3] S.X. Li, F.Y. Zheng, W.L. Cai, A.Q. Han, Y.K. Xie, J. Hazard. Mater. 135 (2006) 431.
[4] S.X. Li, F.Y. Zheng, X.L. Liu, F. Wu, N.S. Deng, J.H. Yang, Chemosphere 61 (2005) 589.
[5] A.E.H. Machado, J.A. de Miranda, R.F. de Freitas, E.T.F.M. Duarte, L.F. Ferreira, Y.D.T. Albuquerque, R. Ruggiero, C. Sattler, L. de Oliveira, J. Photochem. Photobiol. A: Chem. 155 (2003) 231–241.
[6] E. Pepe, O. Abbas, C. Rebufa, M. Simon, S. Lacombe, M. Julliard, J. Photochem. Photobiol. A: Chem. 170 (2005) 143–149.
[7] V. Iliev, J. Photochem. Photobiol. A: Chem. 151 (2002) 195–199.
[8] Z. Xiong, Y. Xu, L. Zhu, J. Zhao, Environ. Sci. Technol. 39 (2005) 651–657.
[9] T.B. Ogunbayo, T. Nyokong, J. Mol. Struct. 973 (2010) 96–103.
[10] E. Marais, R. Klein, E. Antunes, T. Nyokong, J. Mol. Catal. A: Chem. 261 (2007) 36.
[11] K. Ozoemena, N. Kuznetsova, T. Nyokong, J. Mol. Catal. A: Chem. 176 (2001) 29.
[12] K.I. Ozoemena, J. Pillay, T. Nyokong, Electrochem. Commun. 8 (2006) 1391–1396.
[13] J.H. Zagal, S. Griveau, K.I. Ozoemena, T. Nyokong, F. Bedioui, J. Nanosci. Nanotechnol. 9 (2009) 2201–2214.
[14] T. Mugadza, T. Nyokong, Electrochim. Acta 55 (2010) 2606–2613.
[15] W. Freyer, D. Leupold, J. Photochem. Photobiol. A: Chem. 105 (1997) 153–158.
[16] W. Freyer, H. Stiel, M. Hild, K. Teuchner, D. Leupold, Photochem. Photobiol. 66 (1997) 596–604.
[17] W.H. Chen, K.E. Rieckhoff, E.M. Voigt, Chem. Phys. 102 (1986) 193–203.
[18] T.B. Ogunbayo, A. Ogunsipe, T. Nyokong, Dyes Pigments 82 (2009) 422–426.
[19] T.B. Ogunbayo, T. Nyokong, Polyhedron 28 (2009) 2710–2718.
[20] S. Wolfgang, K. Holger, W. Dieter, H. Steffen, R. Beate, S. Gunter, J. Porphyrins Phthalocyanines 2 (1998) 145–158.
[21] D.S. Lawrence, D.G. Whitten, Photochem. Photobiol. 64 (1996) 923–935.
[22] G. Mbambisa, T. Nyokong, Polyhedron 27 (2008) 2799–2804.
[23] J. Liu, A.G. Rinzler, H. Dai, J.H. Hafner, R.K. Bradley, P.J. Boul, A. Lu, T. Iverson, K. Shelimov, C.B. Huffman, F. Rodriguez-Macias, T.Y.-S. Shon, R. Lee, D.T. Colbert, R.E. Smalley, Science 280 (1998) 1253–1256.
[24] T.E. Youssef, Polyhedron 29 (2010) 1776.
[25] L. Ji, F. Liu, Z. Xu, S. Zheng, D. Zhu, Environ. Sci. Technol. 43 (2009) 7870–7876.
[26] L. Ji, Y. Shao, Z. Xu, S. Zheng, D. Zhu, Environ. Sci. Technol. 44 (2010) 6429–6436.
[27] M. Terrones, W.K. Hsu, A. Schwoerer, K. Prassides, H.W. Kroto, D.R. Walton, Appl. Phys. A 66 (1998) 307–317.
[28] Y. Zhang, X. Sun, L. Pan, H. Li, Z. Sun, C. Sun, B.K. Tay, J. Alloys Compd. 480 (2009) L17–L19.
[29] B.K. Price, J.M. Tour, J. Am. Chem. Soc. 128 (2006) 12899–12904.
[30] J. Jiang, R. Saito, A. Grüneis, S.G. Chou, Ge.G. Samsonidze, A. Jorio, G. Dresselhaus, M.S. Dresselhaus, Phys. Rev. B 71 (2005) 205420/1–205420/13.
[31] M.D. Ellison, P.J. Gasda, J. Phys. Chem. 112C (2008) 738–740.
[32] H. Al-Ekabi, N. Serpone, J. Phys. Chem. 92 (1988) 5726–5731.
[33] D.D. Dionysiou, A.P. Khodadoust, A.M. Kern, M.T. Suidan, I. Baudin, J.-M. Laîné, Appl. Catal. B: Environ. 24 (2000) 139–155.
[34] K.J. Laider, J.H. Meiser (Eds.), Sanctuary Physical Chemistry, Fourth ed., Houghton Mifflin Company, Boston, 2003, p. 933.
[35] E. Sibva, M.M. Pereira, H.D. Burrows, M.E. Azenha, M. Sarakha, M. Bolte, Photochem. Photobiol. Sci. 3 (2004) 200–204.
[36] E. Marais, E. Antunes, T. Nyokong, J. Coord. Chem. 61 (2008) 3727.